Magnetic Reconnection Triggering Magnetohydrodynamic Instabilities During a Sawtooth Crash in a Tokamak Plasma

IT Chapman[1], R Scannell[1], WA Cooper[2], JP Graves[2], RJ Hastie[1], G Naylor[1], and A Zocco[1]
[1] *EURATOM/CCFE Fusion Association, Culham Science Centre, Abingdon, Oxon OX14 2DE, UK*
[2] *CRPP, Association EURATOM/Confédération Suisse, EPFL, 1015 Lausanne, Switzerland*

High resolution Thomson scattering measurements with sub-centimetre radial resolution have been made during a sawtooth crash in a fusion plasma in MAST. As magnetic reconnection occurs, a growing magnetic island induces an increase in the temperature gradient at the island boundary layer, before a very rapid collapse of the core temperature. The increase in the local temperature gradient is sufficient to make the plasma core unstable to ideal magnetohydrodynamic instabilities, thought to be responsible for the rapidity of the collapse.

PACS numbers: 52.55Fa, 52.35Py

Magnetic reconnection is the phenomenon of the breaking and rejoining of magnetic field lines in a plasma. Examples of this process are solar flares in astrophysical plasmas [1, 2] and the sawtooth instability in tokamak plasmas [3, 4]. Whilst the sawtooth instability was first observed in 1974 [5], the process by which this periodic collapse of the core plasma temperature occurs is still only partially understood. Detailed diagnosis of the sawtooth crash has shown that the temperature profile is initially essentially axisymmetric, but is then deformed by a helical instability before a very rapid temperature collapse re-establishes an axisymmetric profile with a lower value at the magnetic axis [6, 7].

Tokamak plasmas are susceptible to sawtooth oscillations when the safety factor, $q = rB_\phi/RB_\theta$ is less than unity [8], where r, R are the minor and major radii and B_ϕ, B_θ are the toroidal and poloidal magnetic fields. The helical perturbation which arises during the crash has an $m = n = 1$ structure, where m, n are the poloidal and toroidal periodicity of the wave. The first explanation of the periodic temperature collapses was proposed by Kadomtsev [3], who showed that in the nonlinear regime of the $m = 1$ mode, reconnection occurs at the separatrix on the characteristic Sweet-Parker timescale [1, 2] $\tau_K = \sqrt{\tau_R \tau_A} = \tau_A \sqrt{S}$, where $\tau_A = a\sqrt{4\pi\rho}B_\theta^{-1}$ is the poloidal Alfvén time, $\tau_R = 4\pi a^2/\eta c^2$ is the resistive diffusion time, ρ is the mass density, η is the plasma resistivity and $S = \tau_R/\tau_A$ is the Lundquist number. This timescale is up to two orders of magnitude too large to explain crash times in large modern-day tokamaks, where $\tau_{crash} \sim 20 - 100\mu$s, whereas $\tau_K = 2 - 10$ms.

The three principal observations which any theory must explain are (i) the rapidity of the temperature collapse, (ii) the sudden onset of the collapse and (iii) the incomplete relaxation of the current profile whereby q remains below unity whilst the temperature profile relaxes completely. The onset of the crash represents a theoretical challenge, since the incremental change in the safety factor which governs the stability of the $m = n = 1$ mode is unacceptably small to explain the rapid onset. Many alternative crash models have since been proposed, including resistive two-fluid MHD [9], collisionless kinetic effects [10, 11], accelerated complete reconnection due to nonlinear collisionless effects [12], magnetic stochastization leading to enhanced perpendicular transport [13] and triggering of secondary instabilities [14–16]. Each of these models has had proponents and experimental support. The collisionless reconnection model mediated by the electron pressure gradient [17] provides a satisfactory explanation of the crash rapidity and the sudden onset, but fails to explain the partial reconnection. Similarly, the precipitous drop in the pressure gradient that occurs due to rapid electron heat transport removing the drive for the initial helical perturbation may explain (iii), but not the rapid transition from mode growth to the sudden crash. However, the triggering of a secondary instability [14–16] by the strong pressure gradient arising from the reconnection process, can provide a simultaneous explanation of these phenomena. Recent advances in imaging electron temperature fluctuations with high temporal and spatial resolution [18] suggest that the global stochasticity of the magnetic field [13] is not the dominant crash mechanism since the heat transport exhibits well organised, collective behaviour. Whilst previous experimental data has given great insight into the phenomenology of the crash [7, 18, 19], it had insufficient radial resolution to provide either validation or vitiation of the concept of triggering of secondary instabilities [8, 15, 16], and theoretical or numerical comparison has been stifled by this.

The recently upgraded infrared Thomson Scattering (TS) system on MAST [20], with radial resolution $<$ 10mm and the possibility of temporal resolution of 1μs, has allowed detailed analysis of the electron density and temperature profiles during a sawtooth crash. The system is designed to measure at high spatial resolution and achieve low systematic and random errors, allowing observation of changes in the gradients over narrow regions associated with magnetic islands. Figure 1 shows the electron temperature (T_e) profiles measured by the TS at

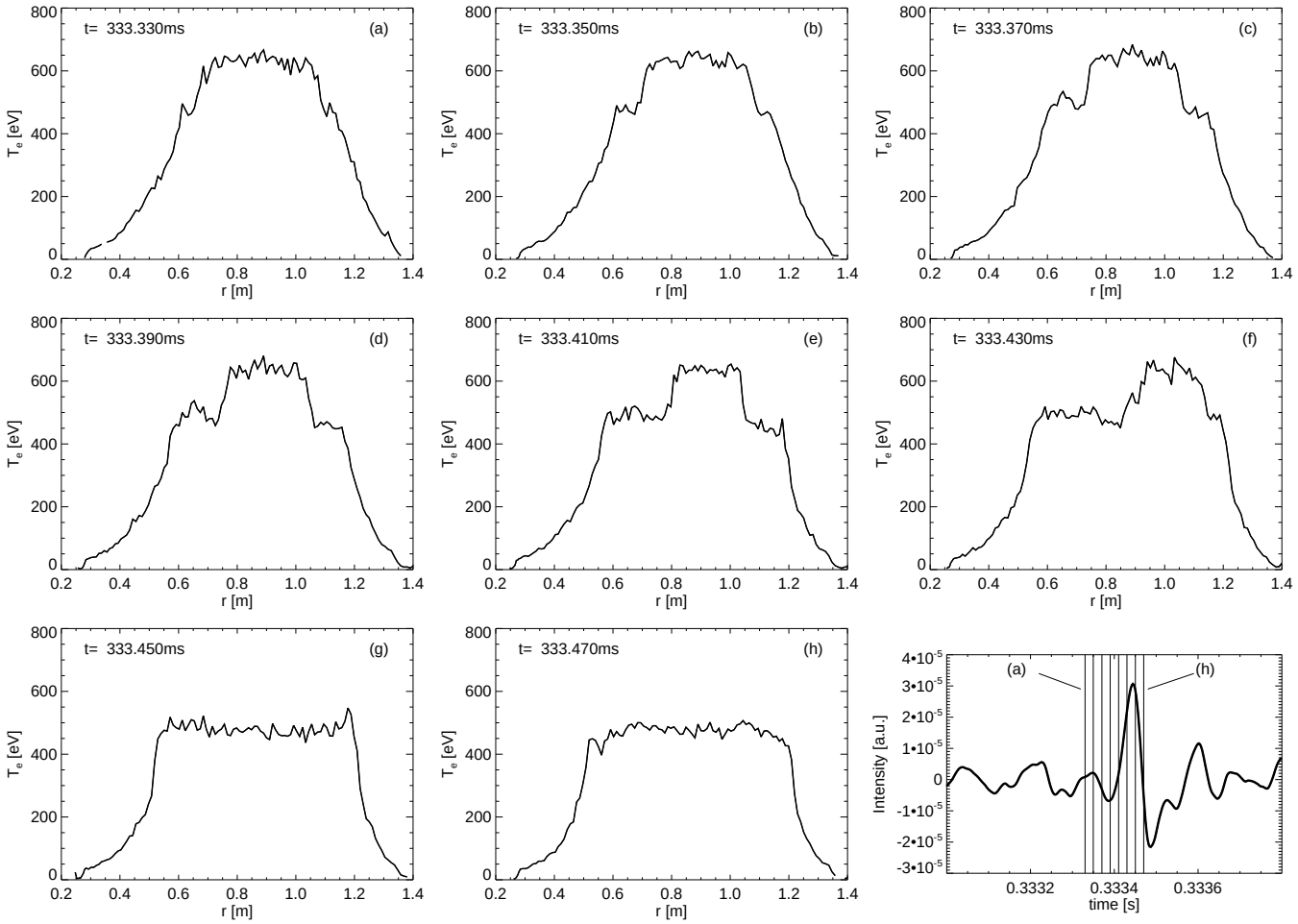

FIG. 1: (a)-(h) show the evolution of the electron temperature profile at every 20μs across a sawtooth crash measured by the Thomson scattering in MAST discharge 24479. Also shown is the n =odd magnetic signals measured by the Mirnov coils on the outboard midplane.

eight time slices, 20μs apart in MAST shot 24479, from the onset of growth of the $m = n = 1$ island until after the sawtooth crash. In this shot, a localised flattening of T_e occurs as an $n = m = 1$ magnetic island develops. Initially the flat-spots are visible on both sides of the magnetic axis in regions where the toroidal magnetic field is strong and weak (eg figure 1(c)) as the diagnostic line-of-sight passes through two parts of the island crescent. Later, the temperature is flattened primarily on the high field side (figure 1(f)) as the island rotates and the TS views through the island O-point. The crash phase occurs between figures 1(f) and 1(g), in less than 20μs. Such local flattening in microsecond timescales was also observed using ECE measurements with 1-2cm radial resolution on DIII-D [21].

In contrast to T_e, the electron density (n_e) profile remains constant during this time, as seen in figure 2. The reason for this is likely to be the relative parallel velocities of the ions and electrons. The electrons have large parallel velocity and so can transport the heat easily,whereas the heavier ions cannot transport the heat on the timescale of microseconds, and so the electron density cannot change or quasi-neutrality would be broken and tend to establish electric fields to restore neutrality. Constant density suggests that full reconnection does not occur, supported by the observation that the safety factor (derived from equilibrium reconstruction with the EFIT code constrained by TS measurements together with magnetic field pitch angle measurements from the motional stark effect diagnostic) remains below unity directly after the sawtooth crash [22].

Both the growth of the magnetic island width and the eventual crash in the temperature profile occur on very rapid timescales, $\sim$100μs and $\leq$20μs respectively. The growth of the island is much quicker than the resistive diffusion time, $\tau_r \sim 180$ms, and the crash occurs on a much faster timescale than expected from reconnection theory [1, 2], $\tau_K \sim 340\mu$s. This rapid evolution of the mag-

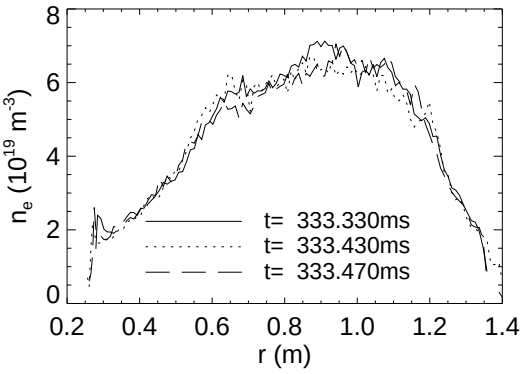

FIG. 2: The electron density profile during MAST shot 24479 remains effectively unaltered whilst on the same timescale figure 1 shows that the electron temperature changes significantly.

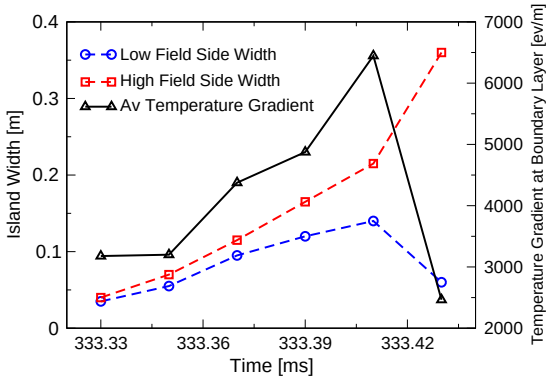

FIG. 3: The Thomson Scattering measurement of the width of the magnetic island on the low- and high-field sides of the magnetic axis together with the electron temperature gradient at the internal boundary layer as the $n = m = 1$ island evolves for MAST discharge 24479.

netic island induces a significant increase in the electron temperature gradient at the island boundary layer, which is consistent with the physical antecedent necessary for triggering a secondary pressure-driven instability [14–16]. The interaction of the electron cross-field thermal conduction and the reconnection of the magnetic field lines associated with the $m = n = 1$ island can increase both the local pressure gradient at the boundary layer adjacent to the reconnecting layer and the poloidal beta of the core ($\beta_p = (2\mu_0 R^2/r_1^4 B_\phi^2)\int_0^{r_1} \mathrm{d}r r^2 \mathrm{d}p/\mathrm{d}r$), which in turn can drive ideal MHD modes on Alfvénic timescales, $\tau_A \sim 0.7\mu$s.. The width of this boundary layer is determined by the ratio of the electron cross-field thermal diffusivity and the speed at which the reconnection progresses [16]. This provides a mechanism whereby the change in the pressure gradient resultant from the presence of the magnetic island causes the internal disruption, rather than the incremental change in the current density profile. Figure 3 shows the evolution of both the width of the island on low- and high-field sides of the magnetic axis, as well as the flux-surface averaged gradient of the electron temperature at the inner island boundary layer as measured by the TS. As the magnetic island width grows, the electron temperature gradient at the boundary layer also increases.

The increase in the local pressure gradient in regions of adverse average curvature drives both ballooning modes [14] and interchange MHD instabilities [15]. The drive from the pressure gradient competes with the stabilising effect of the magnetic shear, $s = r/q\mathrm{d}q/\mathrm{d}r$ and shaping effects [23]. An average stabilising magnetic well exists in shaped tokamak plasmas due to the curvature of the system, except in the region where $q < 1$ where the average curvature is destabilising. In these MAST plasmas, not only does the pressure gradient increase as the island grows, but the radial location of the increased temperature gradient moves towards the magnetic axis (as seen in figure 1), ie towards a region of lower magnetic shear. It should be noted that the increase in the pressure gradient will not give rise to increased diamagnetic or kinetic stabilisation of the interchange mode, since such effects scale with the ion or fast ion pressure gradients respectively, but only the electron temperature changes on these very fast timescales. The ideal Mercier criterion [24] has been calculated for an equilibrium with the temperature profiles for each of the time-slices illustrated in figure 1. The q-profile is obtained from EFIT reconstruction constrained by MSE measurements made shortly before the crash and the pressure gradient is obtained from polynomial fitting of the pressure profile measured by the TS. During the island evolution it is assumed that the plasma core is incompressible, so the enclosed flux in the area of the hot core is the same as it was before the kink perturbation, allowing the safety factor at the boundary layer to be inferred from the pre-island equilibrium. The plasma core shape is taken both from the original equilibrium (labelled 'low δ') and from the (1,1) perturbation produced by axisymmetric linear stability analysis ('moderate δ'). An axisymmetric analysis finds ballooning (figure 4) and ideal Mercier instability (figure 5) by $t = 333.41$ms. The fact that the Mercier index is well above 0.5 suggests that the mode will grow on Alfvénic timescales [25]. Such explosive growth is required to explain the onset of the crash in $\tau_{\mathrm{crash}} \leq 20\mu$s, which is at least an order of magnitude quicker than resistive instability growth or fast magnetic reconnection. Such ideal pressure driven instabilities then cause the strong pressure gradient to propagate towards the axis (since $D_I < 0$ outside $q = 1$) causing the very rapid collapse of T_e [15].

A more accurate non-axisymmetric stability analysis of the kinked equilibrium has been undertaken using the VMEC 3d equilibrium code [26] and the TERPSICHORE

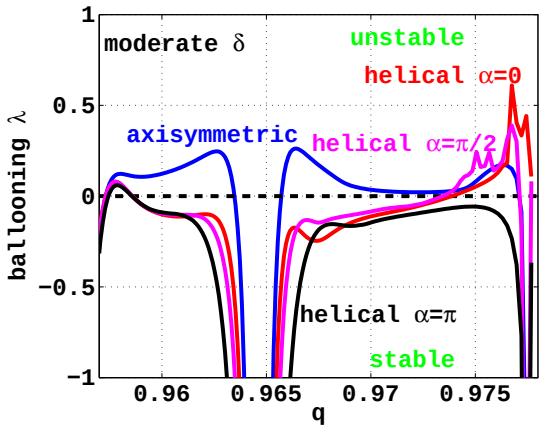

FIG. 4: The infinite-n ballooning mode growth rate of MAST discharge 24479 as a function of q for both 2d and 3d treatment of the plasma core at $t = 333.41$ms. Since the 3d treatment allows for the piling of flux surfaces on the low field side due to the perturbation, ballooning modes become more stable in the core, but are more unstable at the boundary layer.

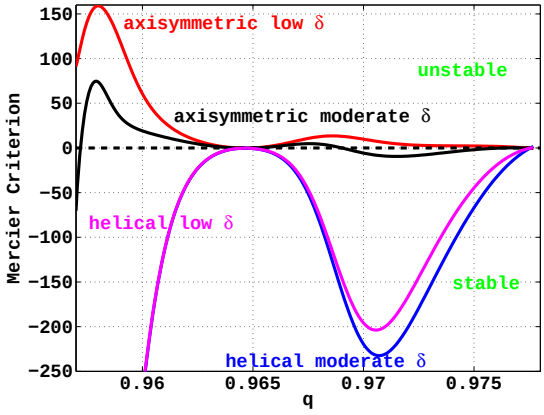

FIG. 5: The Mercier index defined in [24] of MAST discharge 24479 as a function of q for both 2d and 3d treatment of the plasma core at $t = 333.41$ms. Axisymmetric analysis predicts interchange instability for low shaping and marginal stability at the strongest $T_e^{'}$ for moderate shaping whereas helical analysis predicts stability everywhere.

3d linear stability code [27]. When the helical 1/1 perturbation is included, the plasma core becomes stable to ballooning modes except near the boundary layer where instability is exacerbated since the 3d deformation tends to squeeze the pressure gradient outwards. Conversely, in the shaped MAST plasmas, the helical treatment predicts improved Mercier stability, suggesting that ballooning modes represent a stronger candidate to expedite the crash shown in figure 1. Whilst the localised pressure bulges seen experimentally [18] are consistent with ballooning modes, they were sometimes observed to be localised in a region of good curvature, which violates ballooning theory. An explanation could be that the circular plasmas in [18] increased Mercier instability such that interchange modes mediated the rapid crash in this case, whereas ballooning modes mediate these shaped MAST plasmas. Of course, the increased temperature gradient can also give rise to enhanced microtearing instability which would also enhance the heat transport. Nonlinear modelling of mesoscale transport and MHD stability of these MAST plasmas and the interaction of the $m = n = 1$ island with microtearing and macroscopic pressure-driven modes is underway and will be reported in the future.

Finally, it is also possible to estimate the thermal diffusivity of the plasma at the boundary layer from the reconnection speed and the island width. Reference [16] gives that the temperature gradient in the boundary layer for an initial profile of the form $T = T_0(1 - r/r_1)$ is $\mathrm{d}T/\mathrm{d}r'|_{r'=r_1-w} \approx (T_0/r_1)/[(r+\delta)/\delta]$ where r_1 is the minor radius of the $q = 1$ surface, $\delta = \chi_{e\perp}/V_r$ is the thickness of the boundary layer, $\chi_{\perp e}$ is the electron cross-field thermal diffusivity, V_r is the speed of the reconnection and $w = V_r t$ is the incremental width of the island after reconnection begins. By considering the electron temperature gradient illustrated in figure 3, the electron diffusivity is estimated as $\chi_e = 10 - 40\mathrm{m}^2\mathrm{s}^{-1}$ which compares favourably with the coefficients estimated by matching the neutron rate from the experiment in transport simulations or from gyrokinetic simulations [28].

Temperature profile measurements with unparalleled spatial resolution have shed new light on the mechanisms that underlie the sawtooth crash in tokamak plasmas. An $m = n = 1$ magnetic island grows very rapidly leading to a strong increase in the electron temperature gradient outside the island separatrix. The island width grows and the region of increasing gradient moves into regions of lower magnetic shear, before the sawtooth crash occurs in less than 20μs. The sawtooth does not invoke a full magnetic reconnection and the safety factor stays below unity throughout the cycle. The non-axisymmetric plasma in the presence of a growing magnetic island is found to be unstable to interchange or ballooning modes, which are postulated to result in the rapid crash following instability growth on Alfvénic timescales. This supports the hypothesis that the sawtooth occurs due to a pressure-driven magnetohydrodynamic instability triggered by an increase in the electron temperature gradient arising from magnetic reconnection.

The authors acknowledge useful discussions with SC Cowley, CG Gimblett, SD Pinches and A Thyagaraja. This work was partly funded by the United Kingdom Engineering and Physical Sciences Research Council under grant EP/G003955 and the European Communities under the contract of Association between EURATOM and CCFE. The views and opinions expressed herein do not necessarily reflect those of the European Commission.

[1] PA Sweet *Annu Rev. Astron. Astrophys.* **7** 149 (1969)
[2] EN Parker *Astrophys. J., Suppl. Ser.* **8** 177 (1963)
[3] B Kadomtsev *Sov. J. Plasma Phys.* **1** 389 (1976)
[4] RJ Hastie *Astrophysics and Space Science* **256** 177 (1998)
[5] S von Goeler, W Stodiek and N Sauthoff *Phys. Rev. Lett.* **33** 1201 (1974)
[6] AW Edwards *et al Phys Rev. Lett.* **57** 210 (1986)
[7] M Yamada, FM Levinton, N Pomphrey, R Budny, J Manickam and Y Nagayama *Phys. Plasmas* **1** 3269 (1994)
[8] MN Bussac, R Pellat, D Edery and JL Soule *Phys. Rev. Lett.* **35** 1638 (1975)
[9] MN Bussac, D Edery, R Pellat and JL Soule *Plasma Phys. and Controlled Nucl. Fusion Research* (IAEA Vienna) **1** 607 (1976); G Ara *et al Annals of Physics* **112** 443 (1978)
[10] M Kruskal and C Oberman *Phys. Fluids* **1** 275 (1958)
[11] T Antonsen, B Lane and J Ramos *Phys. Fluids* **24** 1465 (1981)
[12] M Ottaviani and F Porcelli *Phys. Rev. Lett.* **71** 3802 (1993)
[13] AJ Lichtenberg, K Itoh, SI Itoh and A Fukayama *Nucl. Fusion* **32** 495 (1992)
[14] MN Bussac and R Pellat *Phys. Rev. Lett.* **59** 2650 (1987)
[15] CG Gimblett and RJ Hastie *Plasma Phys. Control. Fusion* **36** 1439 (1994)
[16] TK Chu *Nucl. Fusion* **28** 1109 (1988)
[17] AY Aydemir *Phys. Plasmas* **4** 3469 (1992); X Wang and A Bhattacharjee *Phys. Rev. Lett.* **70** 1627; 1997 *Phys Plasmas* **4** 1173 (1993)
[18] HK Park *et al Phys. Rev. Lett.* **96** 195004 (2006)
[19] Y Nagayama *et al Phys. Plasmas* **3** 1647 (1996)
[20] R Scannell *et al Rev. Sci. Instrum.* **79** 10E730 (2008)
[21] EA Lazarus *et al Phys. Plasmas* **14** 055701 (2007)
[22] MF de Bock *et al 36th EPS Conference on Controlled Fusion and Plasma Physics* vol 33E, P5.186 (2009)
[23] H Lütjens, A Bondeson and G Vlad *Nucl. Fusion* **32** 1625 (1992)
[24] WA Cooper *Plasma Phys. Control. Fusion* **34** 1011 (1992)
[25] S Gupta, JD Callen and CC Hegna *Phys. Plasmas* **9** 3395 (2002)
[26] SP Hirshman, WI Van Rij and P Merkel *Comput. Phys. Commun.* **43** 143 (1986)
[27] DV Anderson *et al* Int. J. Supercomp. Appl. **4** 34 (1990)
[28] RJ Akers *et al 22nd IAEA Fusion Energy Conference* (Geneva) EX/2-2 (2008)